

Is the cluster environment quenching the Seyfert activity in elliptical and spiral galaxies?

R. S. de Souza^{1*}, M. L. L. Dantas², A. Krone-Martins³, E. Cameron⁴, P. Coelho²,
M. W. Hattab⁵, M. de Val-Borro⁶, J. M. Hilbe⁷, J. Elliott⁸ and A. Hagen⁹,
for the COIN Collaboration

¹MTA Eötvös University, EIRSA “Lendulet” Astrophysics Research Group, Budapest 1117, Hungary

²Instituto de Astronomia, Geofísica e Ciências Atmosféricas, Universidade de São Paulo, R. do Matão 1226, 05508-090, São Paulo, Brazil

³CENTRA/SIM, Faculdade de Ciências, Universidade de Lisboa, Ed. C8, Campo Grande, 1749-016, Lisboa, Portugal

⁴Department of Zoology, University of Oxford, Tinbergen Building, South Parks Road, Oxford, OX1 3PS, United Kingdom

⁵Center for Biomarker Research and Personalized Medicine, Virginia Commonwealth University, Richmond, VA, USA

⁶Department of Astrophysical Sciences, Princeton University, Princeton, NJ 08544, USA

⁷Department of Statistics, School of SFD, Arizona State University, Tempe, AZ, USA

⁸Harvard-Smithsonian Center for Astrophysics, 60 Garden St., Cambridge, MA 02138, USA

⁹Department of Astronomy and Astrophysics, Pennsylvania State University, University Park, PA 16802, USA

Last updated August 14, 2019; in original form 2 August 14, 2019

ABSTRACT

We developed a hierarchical Bayesian model (HBM) to investigate how the presence of Seyfert activity relates to their environment, herein represented by the galaxy cluster mass, M_{200} , and the normalized cluster centric distance, r/r_{200} . We achieved this by constructing an unbiased sample of galaxies from the *Sloan Digital Sky Survey*, with morphological classifications provided by the *Galaxy Zoo Project*. A propensity score matching approach is introduced to control the effects of confounding variables: stellar mass, galaxy colour, and star formation rate. The connection between Seyfert-activity and environmental properties in the de-biased sample is modelled within an HBM framework using the so-called logistic regression technique, suitable for the analysis of binary data (e.g., whether or not a galaxy hosts an AGN). Unlike standard ordinary least square fitting methods, our methodology naturally allows modelling the probability of Seyfert-AGN activity in galaxies on their natural scale, i.e. as a binary variable. Furthermore, we demonstrate how an HBM can incorporate information of each particular galaxy morphological type in a unified framework. In elliptical galaxies our analysis indicates a strong correlation of Seyfert-AGN activity with r/r_{200} , and a weaker correlation with the mass of the host cluster. In spiral galaxies these trends do not appear, suggesting that the link between Seyfert activity and the properties of spiral galaxies are independent of the environment.

Key words: methods: data analysis – methods: statistical – galaxies: clusters: general – galaxies: active – galaxies: Seyfert

1 INTRODUCTION

For a long time it has been argued that active galactic nuclei (AGN) are powered by the accretion of gas into a super-massive black hole (SMBH) located at the centre of its host galaxy (e.g. Lynden-Bell 1969; Magorrian et al. 1998; Orban de Xivry et al. 2011). The AGN-driven energetic outflows, that are launched from the accretion disc surrounding the SMBH, are fundamental processes thought to shape the formation of massive galaxies. In particular, AGN feedback is often invoked in semi-analytic models to explain

the suppression of gas accretion on to the host galaxy and the subsequent quenching of star formation (Birnboim & Dekel 2003; Kereš et al. 2005; Dekel & Birnboim 2006; Somerville et al. 2008; Cattaneo et al. 2009; Kereš et al. 2009; Cattaneo et al. 2011). Empirical evidence supporting the idea that nuclear activity and the evolution of the host galaxy are closely intertwined includes the tight correlation between SMBH mass and the bulge velocity dispersion. The latter is taken to imply a strong connection between the formation and evolution of the central SMBH and that of the bulge (e.g., Ferrarese & Merritt 2000; Gebhardt et al. 2000; Tremaine et al. 2002; Häring & Rix 2004; Somerville et al. 2008; Reines & Volonteri 2015). The AGN feedback interacts with the gas of its host

* E-mail: rafael@caesar.elte.hu

via radiation pressure, winds and jets, hence helping to shape the final mass of the stellar components (Fabian 2012). The AGN feedback can also affect other galaxies in the surrounding environment (Ishibashi & Fabian 2016), with deep implications in the galaxies, groups and cluster evolution. However, a detailed picture of how exactly AGN can affect the evolution of its host remains to be established.

The physical mechanisms that power the AGN are also a matter of debate. Some studies indicate that the dissipation of angular momentum during major mergers might allow gas to accrete into the central black hole (e.g., Hopkins et al. 2006; Kaviraj et al. 2015). Other secular mechanisms, such as disc/bar instabilities, colliding clouds, and supernovae explosions have also been proposed as AGN activity triggers (see Kormendy & Kennicutt 2004; Martini 2004; Jogee 2006; Booth & Schaye 2013, for reviews). Therefore, one should expect to find a correlation between AGN activity and the visual morphology of its host galaxy. This connection has been explored in several studies. For instance, Orban de Xivry et al. (2011) found that the hosts of Narrow-line Seyfert 1 (NLS1) systems tend to be very late-type galaxies, such as grand design spirals, and that NLS1 may represent a different class of AGN in which the black hole growth is dominated by secular evolution much more than their broad-Line Seyfert 1s counterparts. Villarroel & Korn (2014) found differences in the colour distribution and AGN activity of the neighbours to Type-1 and Type-2 AGN and in the fraction of AGN residing in spiral hosts depending on presence or not of a neighbour. It is worth noting that studies as the above implying that different AGN types do not interact in the same way with their environment represent potential issues to the so-called unification AGN model (Antonucci 1993; Urry & Padovani 1995), which suggests that all AGN are the same type of object viewed from a different angle. Alonso et al. (2014) show that spiral galaxies hosting AGN in groups are more likely to be barred than their counterparts in the field. Similar results were presented by Coelho & Gadotti (2011), who found twice as many AGN among barred galaxies, as compared to their unbarred counterparts, for low mass bulges. Nevertheless, Cisternas et al. (2015) claim that the presence of a bar has no influence on the AGN strength, with barred and unbarred active galaxies showing equivalent X-ray luminosity distributions, and Miller et al. (2003) also found that the AGN fraction is independent of the morphological type of the host galaxy, indicating that there is no overall relationship between the star formation activity in the disc component of galaxies and the presence of an AGN. However, Wada (2004) found evidence that mass accretion is not constant during an activity cycle of 10^8 years, but is composed of several shorter episodes. This difference in time-scales may explain the lack of success in finding a correlation between the presence of structures at kpc scales (for example, disc/bar interactions) with the emerging activity in galaxies, except for bright objects such as Quasars (e.g., Moles et al. 1995; Krongold et al. 2001). Finally, Schawinski et al. (2010) found that in early-type galaxies, it is preferentially those with the least massive central black holes that are active, unlike late-type galaxies, in which the most massive black holes are the active ones. Therefore, it is still unclear to what strength the AGN activity is connected to the presence of particular morphological features.

Environmental effects could also turn on or off the AGN activity. Instabilities originating from galaxy mergers, and from interactions between the galaxy and the cluster potential could drive gas towards the galaxy centre, powering the AGN. Notwithstanding, the gas reservoirs of galaxies may be stripped by the tidal field of the group/cluster environment (Larson et al. 1980; Roediger &

Hensler 2005; Roediger et al. 2015, e.g.), by the numerous high-speed encounters with smaller galaxies (e.g., Moore et al. 1996), or by the ram pressure of the intra-cluster gas (Gunn & Gott 1972; Roediger & Hensler 2005; Roediger et al. 2015). The absence of gas to fuel the central black hole would inevitably lead to the turn off of the nuclear activity. Von der Linden et al. (2010) found that the fraction of star-forming galaxies hosting a powerful optical AGN is independent of the normalized cluster-centric distance, r/r_{200} ,¹ indicating that the link between star formation and AGN in these galaxies does not depend on the environment. Nonetheless, the fraction of red galaxies which host a weak optical AGN decreases towards the cluster centre, following the trend of star-forming galaxies. This might indicate that environmental effects gradually quench both the star formation and the AGN activity. More recently Pimblet et al. (2013) using sample of cluster relatively free from mergers, which can locally enhance AGN activity, found a strong relation between AGN activity and r/r_{200} , with significant increase of AGN fraction from the cluster centre to 1.5 Virial radii, with massive galaxies systematically hosting a larger fraction of AGN at any radial location.

Moreover, it is well known that many galaxy properties, such as stellar mass (M_* ; Schawinski et al. 2010), morphology (Dressler 1980; Calvi et al. 2012), star formation rate (SFR; Abraham et al. 1996; Hashimoto et al. 1998; Gómez et al. 2003; Kauffmann et al. 2004; Harris et al. 2016), and optical colours (Strateva et al. 2001; Hogg et al. 2004; Kauffmann et al. 2004; Blanton et al. 2005; Baldry et al. 2006) are strongly correlated with the environment where the galaxy resides. Therefore, the interplay between these competing processes results in a very intricate relation between the AGN activity, galaxy properties and local environment. This requires a careful statistical modelling and the construction of an unbiased sample in order to make robust statistical and, consequently, physical claims.

In this work, we developed a hierarchical Bayesian model (HBM) to explore the roles of morphology, environment, and the occurrence of Seyfert galaxies, f_{Seyfert} . We use a logistic regression methodology, that is a technique designed to deal with binary data (e.g. De Souza et al. 2015b). Additionally, to ease the biases caused by competing effects, we applied a propensity score matching technique (PSM) to build a control sample of inactive galaxies with similar colours ($g-r$), M_* , and SFR.

The outline of this paper is as follows. In Section 2 we provide an overview of the sample selection, the derivation of galaxy and cluster properties, and the selection of the AGN sample via emission line diagnostic diagrams. Section 3 gives a description of the Bayesian statistical methodology. We present our results in depth in Section 4, and, finally, we discuss their physical motivations along with our conclusions in Section 5.

2 CLUSTER SAMPLE

In this section we describe our dataset, which was selected from the updated version of the catalogue compiled by Yang et al. (2007) (communication). The sample comprises groups and clusters of galaxies from the *Sloan Digital Sky Survey* 7th (SDSS-DR7, Abazajian et al. 2009), with additional data retrieved from the SDSS 12th data release database (SDSS-DR12, Alam et al. 2015). We selected

¹ The quantity r_{200} is the radius inside which the mean density is 200 times the critical density of the Universe at the cluster redshift.

all halos within a redshift range of $0.015 < z < 0.1$, having at least 10 galaxy members, and with $13.4 < \log M_{200} < 14.6$, in which M_{200} corresponds to the mass within spheres that are 200 times denser than the critical density of the Universe at the cluster redshift². We included galaxies up to $\sim 10 \cdot r_{200}$ by applying an assignment scheme similar to the one described in Yang et al. (2007) and Duarte & Mamon (2015). As for the M_* and SFR, we adopted the estimated values from Brinchmann et al. (2004). Our sample includes only galaxies brighter than $M_{p,r} < -20.4$, in which $M_{p,r}$ is the k -corrected SDSS Petrosian absolute magnitude in the r -band. This magnitude corresponds to the 95 per cent completeness limit of the sample. The k -corrections were obtained with the `kcorrect` code (version 4_2) described by Blanton & Roweis (2007), choosing as reference the median redshift of the SDSS main galaxy sample ($z = 0.1$). All the criteria described above leads to a sample of 32,353 galaxies within 1,122 groups and clusters.

We also split the sample into two groups, ellipticals and spirals, in order to avoid the oversimplified characterization of the AGN host galaxies as a single class, but rather understand how the galaxy-AGN co-evolution varies between morphologies (Schawinski et al. 2010). This also helps to account for the well known morphology- r/r_{200} relation, in which spirals tend to be mainly located in the outskirts of their respective groups or clusters, whereas ellipticals can be found specially in their inner parts towards regions of increasing local galaxy density (e.g. Goto et al. 2003). The morphological typing relies in the visual classification scheme performed by citizen scientists from the *Galaxy Zoo Project* (Lintott et al. 2008). We use the definition of clean sample of Land et al. (2008), which requires at least 80 per cent majority agreement on the morphology of any object. For the analysis, we place all clusters into a common scale (i.e. r_{200}) to form a composite sample in order to minimize radial sampling bias due to variations in cluster richness (e.g. Barkhouse et al. 2009, and references therein).³

2.1 AGN selection

The classification of objects in our sample is based on the diagram introduced by Baldwin et al. (1981), hereafter BPT [but see also Veilleux & Osterbrock (1987); Kewley et al. (2001); Kauffmann et al. (2003); Stasińska et al. (2006); Schawinski et al. (2007)], as shown in Figure 1, and is available for galaxies with the emission lines $H\beta$, [OIII], $H\alpha$, [NII] for which the signal to noise ratio $S/N > 1.5$. The Star Forming galaxies are those whose emission lines are partially or fully dominated by star formation in the diagram as defined by the theoretical extreme starburst line of Kewley et al. 2001. Composite objects are the ones falling between this extreme starburst line and the empirical pure starburst line of Kauffmann et al. (2003). These are objects that are constituted by co-existing/competing star formation and nuclear activity in terms of ionizing luminosity strength. On the right side of the Kewley et al. (2001) line reside the galaxies whose emission lines are dominated by sources of ionization other than young stars, which are empirically divided into two major AGN sub-classes, the lower branch of low-ionization narrow emission-line regions (or LINERs) and the upper branch of Seyfert galaxies delimited by the line derived by Schawinski et al. (2007). This leads to a classification of objects

in our sample as Star Forming, Seyfert, LINER, and Composite as displayed in Fig. 1, where we show the positions of all galaxies in the sample on the BPT diagram.

Nonetheless, the nature of LINERs, as low-luminosity AGN, is still uncertain and there is a growth of evidence indicating that the majority of galaxies with such spectra classification is unlikely to be true AGN (see e.g., Stasińska et al. 2008; Schawinski et al. 2010; Singh et al. 2013). Many of them may actually be retired galaxies powered by old stellar populations (Maraston 2005; Cid Fernandes et al. 2010; Stasińska et al. 2015). Due to this uncertain nature of LINER galaxies, and with the intent to reduce contamination from false-negative AGN in objects belonging to the Composite region, we chose to eliminate most of them from our analysis, but allowing a narrow region around the Kauffmann et al. (2003) curve ($\Delta \log([NII]/H\alpha) \lesssim 0.05$) to accommodate inherent uncertainties in the curve definition. This allows us to retain only the clearly distinct AGN and non-AGN host galaxies in this study, following an approach similar to the one employed by Schawinski et al. (2010).

2.2 Control sample

Galaxies hosting AGN have different characteristics from their inactive counterparts, preferentially populating the so-called *green valley* and *red sequence* of the colour-mass diagram (e.g. Smolčić 2009; Schawinski et al. 2010). Additionally, in recent years, there has been an ongoing discussion regarding AGN feedback and the connection with SFR: it is believed that AGN activity suppresses the formation of new stars (Page et al. 2012; Booth & Schaye 2013; Bluck et al. 2014; Li et al. 2015). Given that spirals are usually rich in gas and dust, and consequently have high levels of SFR, it is possible to observe a peak of SFR in spirals that do not host AGN. Moreover, the distribution of galaxy colours is linked to the SFR distribution: bluer galaxies possess younger stellar populations, whereas spirals which host AGN are redder and have older stellar populations. These trends can be seen in our sample, both in the colour-mass and colour-SFR diagram in the top and bottom panels of Fig. 2, respectively. The galaxies hosting Seyfert-AGN (orange dots) are compared against inactive galaxies in the sample represented by the bulk of grey dots.

To mitigate this bias, mostly due to the spirals, we built a control sample of inactive galaxies (i.e. those under the curve described by Kauffmann et al. 2003) by matching each pair Seyfert/non-Seyfert galaxy against the confounding covariates, $X_c = \{M_*, (g-r), SFR\}$, and their morphological type⁴. The match is performed via a non-parametric approach known as propensity score matching (PSM, Ho et al. 2007; Austin 2011) using the `MATCHIT` R package (Ho et al. 2011). For each Seyfert galaxy, the method searches for the closest inactive galaxy, in the multidimensional space formed by X_c , via a k -nearest neighbourhood algorithm (see e.g. §3.1; Ishida & de Souza 2013, for a review); the results are presented in Fig. 3. After the PSM, the distributions of the active and inactive sample closely resemble each other and any potential effect that X_c may have on the presence of a Seyfert-AGN is subsumed, since X_c is virtually held constant within each pair of galaxies. The final de-biased sample is composed by 1,744 objects

² All reported masses are in Solar mass units, but suppressed from the text for simplicity.

³ A detailed description of the construction of the entire dataset is available in Trevisan et al. (2016).

⁴ Although $(u-r)$ is the most commonly used SDSS colour to characterize galaxies through the colour-mass diagram (e.g. Strateva et al. 2001; Baldry et al. 2004, 2006), we chose to use the optical colour $(g-r)$ due to the ageing effects and processes suffered by the u band, which can be non-negligible for SDSS-DR7 data (see e.g. Doi et al. 2010).

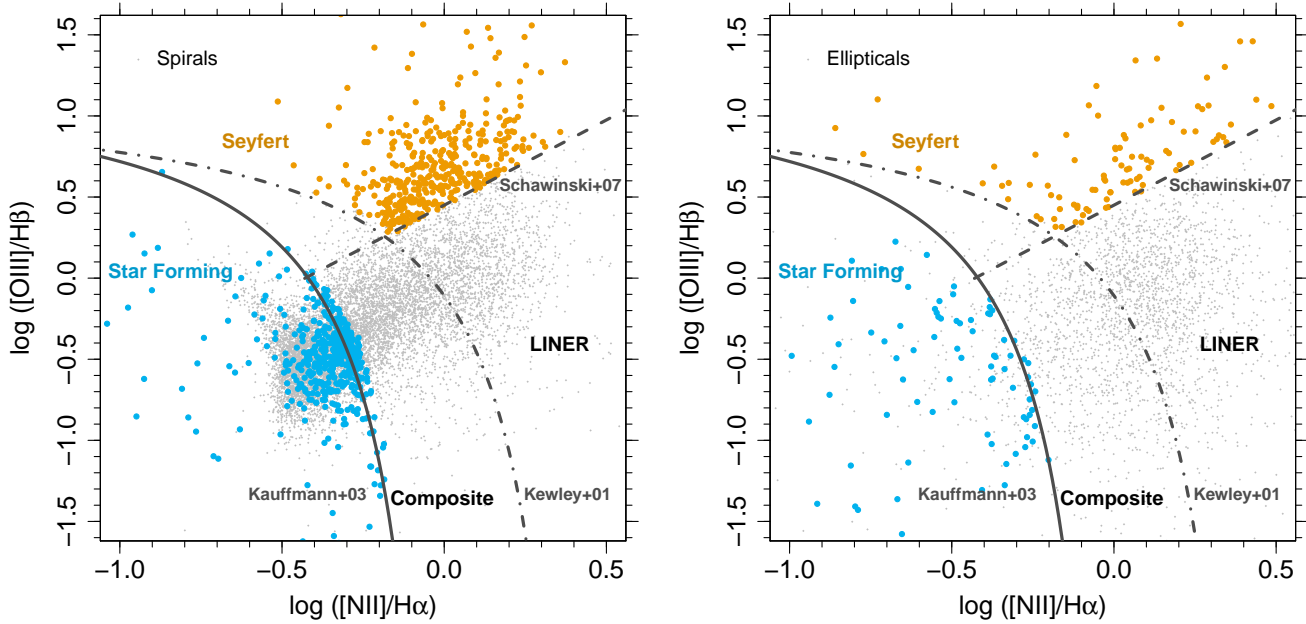


Figure 1. BPT plane for our galaxy sample for both spirals (left panel) and elliptical galaxies (right panel). The vertical-axis represent the ratio of $[\text{OIII}]/H\beta$, while the horizontal-axis is the ratio of $[\text{NII}]/H\alpha$. The grey dots represent the entire galaxy sample, the orange dots are the Seyfert galaxies, and the blue points represent the control sample of inactive galaxies selected with the propensity score matching (see Sec. 2.2). The solid curve is the Kauffmann et al. (2003) line: galaxies above the curve are designated AGN, those below are regular star-forming galaxies. The dot-dashed line represents the Kewley et al. (2001) curve, where galaxies between the Kauffmann et al. and Kewley et al. curves are defined as composites: weaker AGN whose hosts are also star-forming galaxies. The dashed line is the Schawinski et al. (2007) curve, which separates LINER and Seyfert objects.

from which 492 are ellipticals and 1,252 are spirals. The subset is displayed in the BPT diagram (Fig. 1) as follows: cyan dots represent the control sample; the orange ones, the active sample. In the following section, we describe how to build a Bayesian model to explore the effects of r/r_{200} and M_{200} in our de-biased sample.

3 BAYESIAN LOGISTIC MODEL

The simple *linear regression* model has long been a mainstay of astronomical data analysis (e.g. Isobe et al. 1990; Feigelson & Babu 1992; Kelly 2007; Sereno 2016). One important example is the determination of the line of best fit through Hubble’s diagram (Hubble 1929; Abraham & van den Bergh 2001, more recently). Nonetheless, the assumptions of the linear model fall short when the data to be modelled come from *exponential family* distributions other than the Normal/Gaussian⁵ (Hardin & Hilbe 2012; Hilbe 2014). For such problems, there is an overarching solution known as generalized linear models (GLMs). Regression models in the class of GLMs, first developed by Nelder & Wedderburn (1972), take a more general form than in ordinary linear regression:

$$\begin{aligned}
 Y_i &\sim f(\mu_i, a(\phi)V(\mu_i)), \\
 g(\mu_i) &= \eta_i, \\
 \eta_i &\equiv \mathbf{x}_i^T \boldsymbol{\beta} = \beta_0 + \beta_1 x_1 + \dots + \beta_k x_k.
 \end{aligned}
 \tag{1}$$

⁵ The exponential family comprises a diverse set of common distributions describing both continuous and discrete random variables (e.g., Gaussian, Poisson, Bernoulli, Gamma, etc.)

In equation (1), f denotes a response variable distribution from the exponential family (EF), μ_i is the response variable mean, ϕ is the EF dispersion parameter in the dispersion function $a(\cdot)$, $V(\mu_i)$ is the response variable variance function, η_i is the linear predictor, $\mathbf{x}_i^T = \{x_{i1}, x_{i2}, \dots, x_{ik}\}^T$ is a vector of explanatory variables (covariates or predictors), $\boldsymbol{\beta} = \{\beta_1, \beta_2, \dots, \beta_k\}$ is a vector of covariate coefficients, and $g(\cdot)$ is the link function, which connects the mean to the linear predictor η . If the response is Gaussian, then $f = \text{Normal}$, $g(\mu) = \mu$, $a(\phi) = 1$, $V(\mu) = \sigma^2$, and the general form of the GLM recovers the ordinary linear regression as a special case:

$$\begin{aligned}
 Y_i &\sim \text{Normal}(\mu_i, \sigma^2), \\
 \mu_i &= \beta_0 + \beta_1 x_1 + \dots + \beta_k x_k.
 \end{aligned}
 \tag{2}$$

To date, there has been only a handful of astronomical studies applying GLM techniques, such as logistic (e.g., Raichoor & Andreon 2012, 2014; De Souza et al. 2015a), Poisson (e.g., Andreon & Hurn 2010), gamma (Elliott et al. 2015), negative binomial (De Souza et al. 2015b), and Normal regressions (Bhardwaj et al. 2016; Lenz et al. 2016). The methodology discussed herein focuses on logistic regression, which is suitable for handling Bernoulli (or binomial) distributed data. The Bernoulli distribution describes a process in which there are only two possible outcomes: success or failure (yes/no, on/off, red/blue, etc.; typically coded as 1/0). Bernoulli distribution is a particular case of the more general binomial distribution, $\text{Binomial}(n, p) = \binom{n}{y} p^y (1-p)^{n-y}$, for which y is the number of successes ($y = 1$), n is the number of trials, and p is the probability of success. For the Bernoulli distribution, $\text{Bernoulli}(p) = p^y (1-p)^{1-y}$, the number of trials, n , is set to 1. The link function (Eq. 3) derives directly from the underlying Bernoulli probability distribution and ensures a bijection between

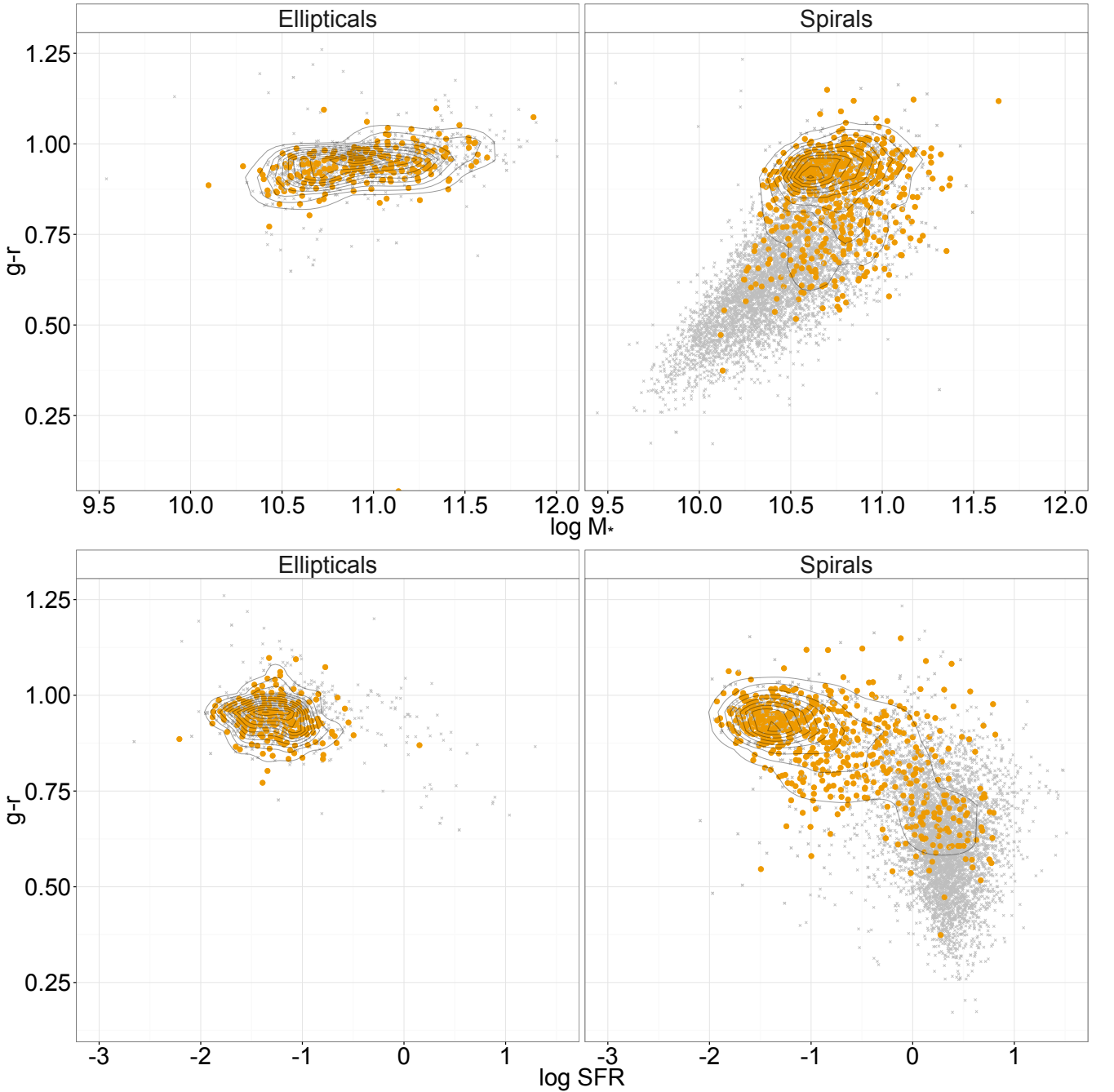


Figure 2. Distribution of the Seyfert-AGN (orange dots) on the $(g-r)$ colour-mass (top panel), and colour-star-formation (bottom panel) diagrams. Left panels: elliptical galaxies; right panels: spiral galaxies. The grey dots represent the whole galaxy population, on top of which we plot the Seyfert hosts, with accompanying grey contour levels of the Seyfert-population.

the $(-\infty, \infty)$ range of the linear predictor, η , and the $(0,1)$ range of non-trivial probabilities for the binomial population proportion (the Bernoulli p). The natural link function for the Bernoulli distribution is known as the logit link, which defines the logistic model:

$$g(p) = \text{logit}(p) \equiv \log\left(\frac{p}{1-p}\right). \quad (3)$$

The logit function has another desirable property: that the exponentiated coefficients of the linear predictors can be naturally inter-

preted in terms of an odds-ratio gradient, $\frac{p}{1-p}$ (e.g. the relationship between the odds-ratio of AGN activity and distance to the cluster centre). As for our analysis we employed an important extension of the GLM methodology known as generalized linear mixed models (GLMMs; Hilbe 2009). The GLMM model, in our context, accounts for variations in the intercept and slopes β_{ij} :

$$\eta_{ij} = \beta_{1,j} + \beta_{2,j}x_1 + \dots + \beta_{k,j}x_k, \quad (4)$$

where the index j represents the different galaxy morphologies. There are a few key advantages in this more general methodology

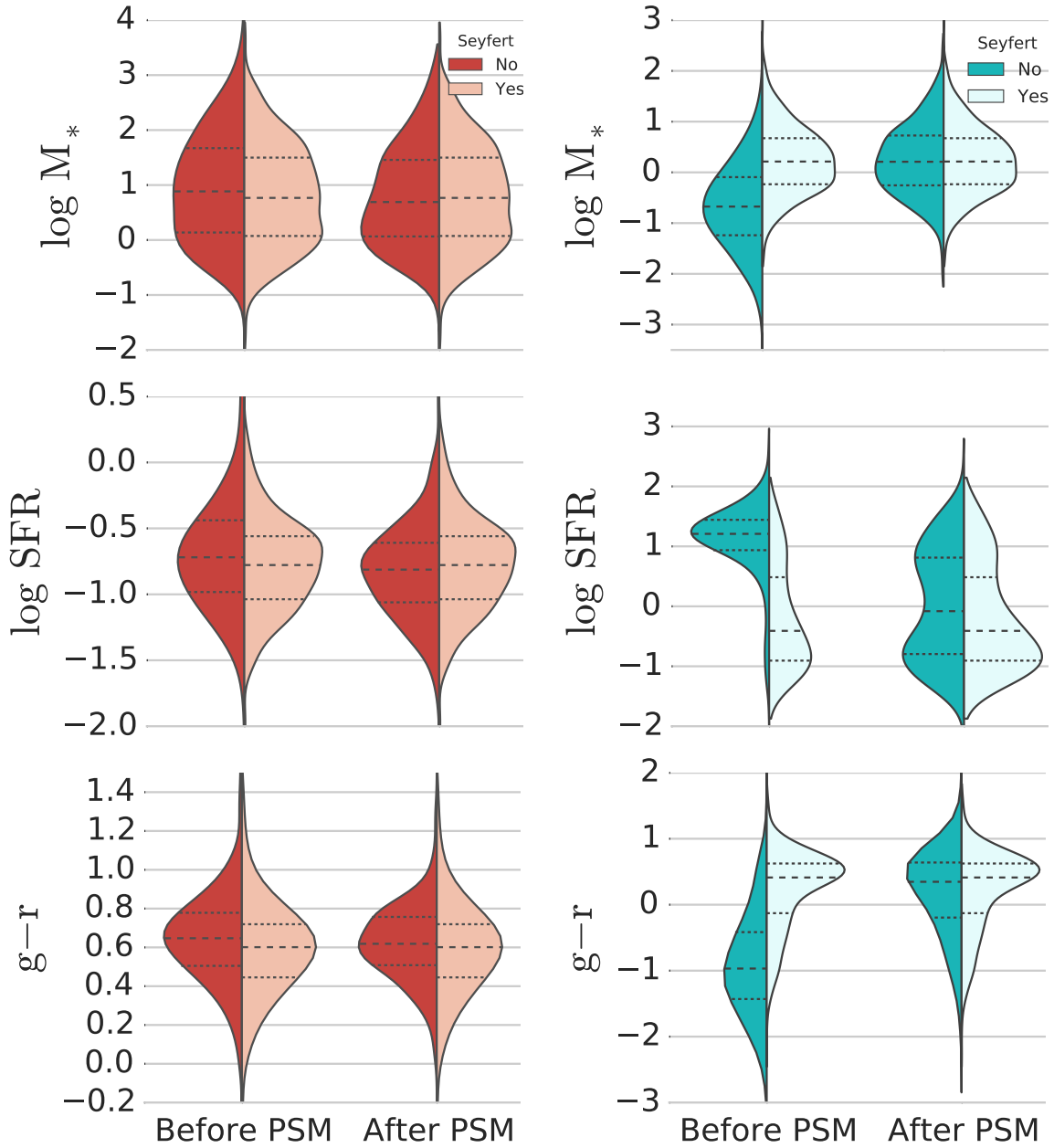


Figure 3. Distribution of $\log M_*$, $\log \text{SFR}$, and the $(g-r)$ colour for elliptical (left column, in red) and spiral (right column, in cyan) galaxies. In each representation, the right and left distributions represent respectively the samples with and without Seyfert AGN activity, portrayed by an asymmetric violin plot. The dotted and solid lines in each violin represent the median and 95 per cent quantiles of the sample, while the shape, denotes its probability distribution. Note that all variables are standardized, for illustrative purposes, as follows, $x^* = (x - \hat{\mu}_x) / \hat{\sigma}_x$, for x^* is the standardized variable (vertical axis), and $\hat{\mu}_x$ and $\hat{\sigma}_x$ represent its sample mean and standard deviation respectively.

when compared to the standard approaches. Classical estimation, which separates the information of each group in sub-samples, can be useless if the sample size in a given group is too small. On the other hand, if a classical regression is applied ignoring group indicators, the results can be misleading by ignoring group-level variation. GLMMs, also known as multilevel modelling, represent a compromise between the overly noisy analysis of each group independently and the oversimplified approach that ignores group indicators (Gelman & Hill 2007). A foremost reason to prefer a GLMM model over a standard logistic model relates to the lack of independence between observations when galaxy morphologies are con-

sidered as groups. A basic logistic model, whether estimated using maximum likelihood or by using Bayesian methods assumes the independence between each observation in the model. When the data are grouped into levels based on galaxy morphology, this adds extra correlation into the model. A GLMM adjusts for the within-morphology correlation, and therefore is the suitable model for this data.

The analysis of this work is performed using the Just Another

Gibbs Sampler (JAGS)⁶ package, a program for analysis of Bayesian models using a Markov Chain Monte Carlo (MCMC) framework. We initiate three Markov chains by starting the Gibbs sampler at different initial values sampled from a Normal distribution with zero mean and standard deviation of 100. The initial burn-in phases were set to 20,000 steps followed subsequently by 50,000 iteration steps, which are sufficient to guarantee the convergence of each chain via the so-called Gelman-Rubin statistics (Gelman & Rubin 1992).

4 DEPENDENCE OF SEYFERT ACTIVITY WITH CLUSTER PROPERTIES

To model the presence or absence of Seyfert galaxies, f_{Seyfert} , we apply a Bayesian logistic regression. The predictor variables reflecting the environment where the galaxy resides and the host cluster property are r/r_{200} , and $\log M_{200}$ ⁷. The r/r_{200} works as a proxy for the local density measure, but can be also understood as a time-scale, given its relationship to the time since the galaxy infall into the cluster began (Gao et al. 2004) (modulo a small proportion of ‘backsplash’ galaxies; Pimbblet 2011). This time-scale is also connected with processes that quench star formation in galaxies. For instance, long-time scale interaction processes, such as strangulation or harassment, would be effective over the entire radial range, while shorter time scale processes, such as ram pressure, would be more localized near the centre, where the density of the gas is higher (Von der Linden et al. 2010).

Our model simultaneously accounts for the dependence of f_{Seyfert} on r/r_{200} , $\log M_{200}$, and galaxy morphology. The model is portrayed as a graphical model in Fig. 4, and reads as follows: each galaxy in the dataset, composed of N objects, has its probability of hosting a Seyfert-AGN described by a Bernoulli distribution whose probability of success, $p \equiv f_{\text{Seyfert}}$, relates to r/r_{200} , and $\log M_{200}$ through a logit link function (to ensure the probabilities will fall between 0 and 1) and the linear predictor

$$\eta = \beta_{1,j} + \beta_{2,j} \cdot \log M_{200} + \beta_{3,j} \cdot r/r_{200}, \quad (5)$$

where j is an index representing if a galaxy is elliptical or spiral. We assume non-informative priors for the coefficients β_1 , β_2 , β_3 , where we assumed Normal priors with mean μ and standard deviation σ for which we assign shared hyper-priors $\mu \sim \text{Normal}(0, 10^3)$ and $1/\sigma^2 \sim \text{Gamma}(10^{-3}, 10^{-3})$ ⁸. By employing a hierarchical Bayesian model for the varying coefficients β_j , we allow the model to borrow strength across galaxy types. This happens via their joint influence on the posterior estimates of the unknown hyper-parameters μ and σ^2 . Thus, the mixed model herein employed can be understood as a compromise between an analysis that does not account for the information regarding different galaxy morphologies (e.g., Fig. 7; Pimbblet et al. 2013), and the one which splits the data into independent slices (e.g. Fig 12; Von der Linden et al. 2010). The former implicitly assumes a pooled estimate (e.g., Gelman & Hill 2007), i.e. both galaxy types are sampled from the same common distribution ignoring any possible variation among them. The later represents an independent analysis for each class, making

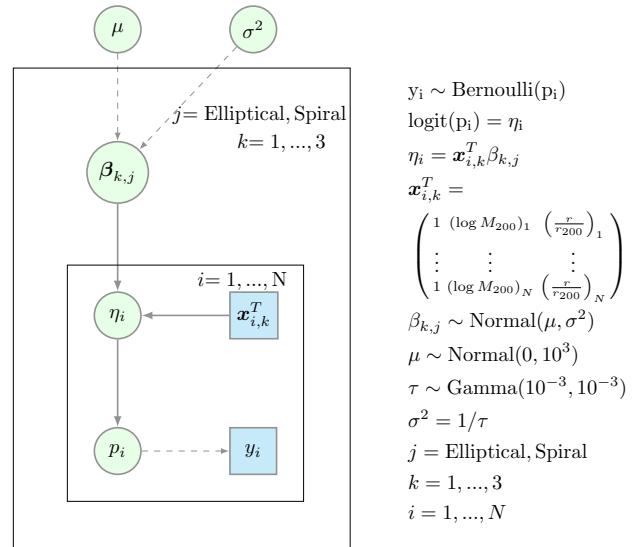


Figure 4. A graphical model representing the hierarchy of dependencies for a data set of galaxies indexed by the subscript i . The dashed arrows represent stochastic dependencies, while straight arrows show the systematic ones. Blue square represents input data, and green circles are model parameters.

the assumption that each morphological type is sampled from independent distributions. Our GLMM, on the other hand, allows us to account for the differences between elliptical and spiral hosts in an integrated fashion.

Furthermore, by modelling the data on its natural scale (i.e. as a binary variable), our model does not require any arbitrary data binning, and our predicted fractions of AGN are always physically meaningful, even if extrapolated. Such features cannot be achieved by standard linear fitting methods. We refer the reader to appendix B for the full script explaining how to implement the model in JAGS.

The fitted coefficients are displayed in Tab. 1; in Fig A1, we present their posteriors. To visualise how the model fits the data, we display, in Fig. 5, the predicted probabilities f_{Seyfert} as a function of r/r_{200} in slices of $\log M_{200}$. For each slice, we present the stacked data, for illustrative purposes, and the fitted model and uncertainty. The shaded areas represent 50 per cent, and 95 per cent probability intervals. We recall that the fitting was performed without making use of any data binning. The simple linear model, in the linear predictor scale, is flexible enough to fit the data well, without the need of non-linear dependencies.

The coefficients for the logit model represent the log of the odds ratio for Seyfert activity. Since the predictors are scaled, it allows us to perform a relative comparison between variables measured in different units. For example, $1\text{-}\sigma$ variation in the r/r_{200} (≈ 2) towards the cluster outskirts for an elliptical galaxy residing in a cluster with an average mass $\log M_{200} = 14$ produces on average a change of 0.197 in the log of odds ratio, or in other words it is 21.7 per cent more likely to be a Seyfert galaxy. Likewise, an elliptical galaxy at an average r/r_{200} (≈ 2.2) residing in a cluster with $\log M_{200} = 14.5$ is ≈ 15.5 percent less likely to be a Seyfert galaxy than a similar galaxy residing in a cluster with $\log M_{200} = 14$. Unlike elliptical galaxies, spirals are virtually unaffected by the position inside the cluster or the mass of its host, with all the fitted coefficients being consistent with zero.

⁶ <http://CRAN.R-project.org/package=rjags>

⁷ We standardized the predictors before the analysis in order to improve possible collinearity and scaling bias due to units differences.

⁸ The inverse Gamma prior accounts for the fact that the variance is always positive.

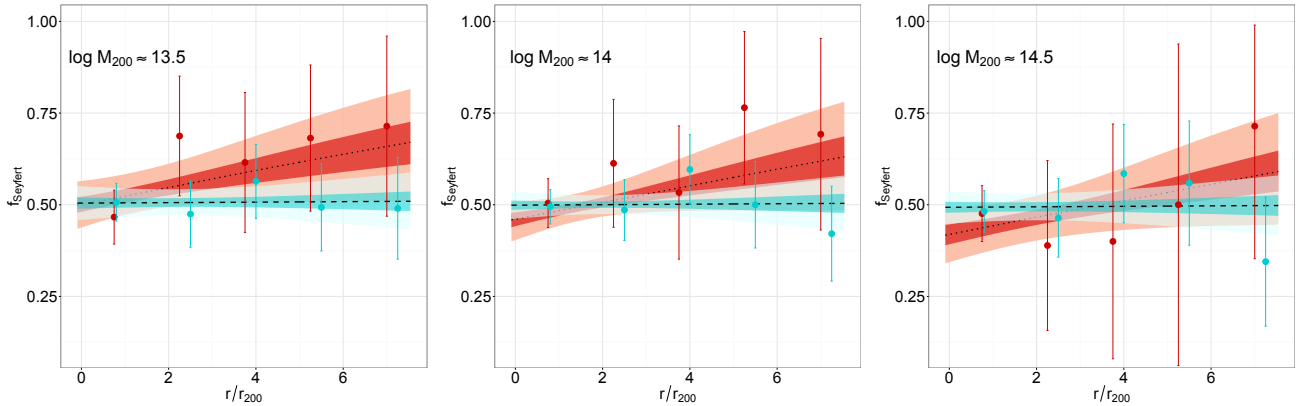


Figure 5. Two-dimensional representation, in slices of $\log M_{200}$, of the six-dimensional parameter space describing the dependence of Seyfert-AGN activity as a function of r/r_{200} , and $\log M_{200}$ for spirals, and elliptical galaxies. In each panel the black lines represents the posterior mean probability of Seyfert-AGN activity for each value of r/r_{200} , while the shaded areas depicts 50 per cent, and 95 per cent probability intervals. Galaxy types are colour-shape-coded as follows: Ellipticals (red shaded area, dotted line), spirals (green shaded area, dashed line). Data points with error bars represent the binned data (slightly shifted along the x -axis for clarity) for purely illustrative purposes.

Table 1. Estimated β_i coefficients from the Bayesian logistic regression analysis for ellipticals and spirals galaxies. The ΔOdds represents the expected change in the odds of Seyfert activity by a variation of $1-\sigma$ in the predictor variables, while holding the another at their mean.

	Galaxy Morphological Type			
	Ellipticals		Spirals	
	β_i	ΔOdds	β_i	ΔOdds
Intercept	0.049 ± 0.088		0.003 ± 0.052	
$\log M_{200}$	-0.169 ± 0.094	-15.5%	-0.024 ± 0.052	-2.4%
r/r_{200}	0.197 ± 0.115	21.7%	0.006 ± 0.054	0.6%

5 DISCUSSION AND FINAL REMARKS

We study how Seyfert-AGN activity in elliptical and spiral galaxies depends on local and global cluster properties, herein represented by the cluster-centric distance and the mass of the galaxy cluster. For such, we used a sample of low redshift clusters ($0.015 < z < 0.1$), with at least 10 galaxy members each, and with $13.4 < \log M_{200} < 14.6$, from which we include galaxies up to $10 \cdot r_{200}$. It is worth to stress that previous studies have mostly considered only very massive clusters, while the present work extends the analysis to the lower-end of the cluster mass function.

We found that f_{Seyfert} in elliptical galaxies strongly depends on the r/r_{200} , whereas no dependence is seen to occur for the spiral hosts. The deficit of AGN towards the cluster centre is in agreement with previous investigations (e.g. [Gilmour et al. 2007](#); [Pimblet et al. 2013](#)), and might be explained by the fact that galaxies in cluster centres should be more stripped of cold gas that can serve as a fuel for AGN activity ([Lietzen et al. 2011](#); [Pimblet et al. 2013](#)). Previous studies have shown that conditions in the central regions of clusters are inhospitable for AGN activity even for galaxies in pairs interactions. The proximity to the cluster centre may induce decreases in AGN activity by limiting gas availability, most likely of cold gas, around the galaxy ([Khabiboulline et al. 2014](#)). This may be caused by the ram pressure stripping ([Fujita 2004](#); [Roediger & Hensler 2005](#); [Roediger et al. 2015](#)), which for ellipticals may be considerably important, sweeping out the residual gas content of these galaxies, hence starving the central SMBH as consequence ([Schawinski et al. 2007](#); [Booth & Schaye 2013](#); [Li et al. 2015](#)). This is also consistent with the recent finding of [Boselli et al.](#)

(2014), that using a volume-limited sample of nearby objects found evidence that ram pressure truncates the infall of pristine gas from the halo, being the dominant process driving the evolution of galaxy clusters.

Nonetheless, a puzzle still remains: why spirals are not affected in the same way? We argue that the reason might be a consequence of the extra gravitational force provided by their bulges, which dominates the holding force in the central few kpc (see e.g. the N -body simulations from [Abadi et al. 1999](#)). This is also consistent with the more recent results from a hydrodynamical simulation, which includes both mechanical and radiative AGN feedback, from [Shin et al. \(2012\)](#), which shows that the AGN activity is less affected by gas stripping than the SFR, because the SMBH accretion is primarily dominated by the density of the galaxy central region. This phenomenon may be related to the observational findings of e.g. [Schawinski et al. \(2010\)](#), suggesting different characteristics for the evolution of SMBH within spirals and ellipticals. This might be linked to the positive correlation between the mass of the bulge and the mass of the central SMBH in spirals galaxies ([Ferrarese & Merritt 2000](#); [Häring & Rix 2004](#); [Somerville et al. 2008](#); [Reines & Volonteri 2015](#)), which provides the extra potential well in the few central kpc. Thus, the spirals might be capable of holding the internal reservoir of gas independently of environment effects, thus keeping the fraction of nuclear activity nearly constant throughout their position inside the cluster.

Our analysis and results can be summarized as follows:

- To control for effects of confounding variables, we built a control sample of inactive galaxies matching each pair against their M_* , $(g-r)$, and SFR, hence allowing us to make cleaner claims about causal effects;
- The Bayesian logistic model does not need to rely on arbitrary data binning, providing the proper scale for modelling a binary variable (presence/absence of Seyfert). Therefore allowing an intuitive interpretation of the fitted coefficients, and unbiased results when compared to standard Gaussian approaches;
- The odds of Seyfert-AGN in elliptical hosts increases towards the group/cluster outskirts by a factor of ~ 21 per cent for one- σ increase of r/r_{200} , in clusters with an average mass of $\log M_{200} \approx 14$, and the effect is more prominent in more massive clusters;
- The mixed model used in this work accounts for the differ-

ences between elliptical and spiral galaxies into an integrated fashion, borrowing strength across sub-samples;

- The f_{Seyfert} in spirals are virtually unaffected by the external environment. We argue that this can be a consequence of the spirals being able to hold an internal reservoir of gas, and this might be caused by some type of protection provided by the galaxy's disc or by extra gravitational force provided by their central regions.

- An alternative scenario for our findings may represent a challenge for the unified AGN model. The different behaviour of AGN in spiral and elliptical hosts may indicate that not all AGN are the born same, and may depend of their surrounding environment. This is consistent with Villarroel & Korn (2014), who found differences in the host morphologies behaviour of Type-1 and Type-2 AGN and indicatives for two distinct classes. An interesting puzzle that shall be addressed in a follow-up investigation.

Generalized linear models are a cornerstone of modern statistics, but nearly *Terra incognita* in astronomical investigations. In the present work, we employed a Bayesian logistic mixed model designed to represent binary data, to analyse the probability of Seyfert-AGN activity as function of their position inside the group/cluster and the mass of its host. Standard approaches in the literature applying a classical linear regression in a fractional data (e.g. fractions of AGN per bin of r/r_{200}) do not have any restriction requiring the prediction fractions to fall between 0 and 1, and cannot be extrapolated while still providing meaningful results. The combination of a propensity score matching and a Bayesian logistic mixed regression allow us to model the f_{Seyfert} with an unparalleled statistical robustness up to date.

Finally we are able to answer the question posed in the title: *Is the cluster environment quenching the Seyfert activity in elliptical and spiral galaxies?* In elliptical galaxies, yes. The regions towards the cluster centre are hostile to the central SMBH residing in these galaxies. On the other hand, spirals appear to be spared and they seem to keep feeding their AGN while falling into the cluster potential.

ACKNOWLEDGEMENTS

This work is a product of the 2nd COIN Residence Program. We thank Alan Heavens and Jason McEwen for encouraging the realization of this edition. We thank E. E. O. Ishida, L. Dobos, R. Beck, B. Kocsis, and B. Villarroel for the fruitful discussions and suggestions. A particular thank goes for M. Trevisan for kindly providing the dataset used in this work and for participating in several discussions. We thank the anonymous referee for the constructive suggestions and comments. The program was held in the Isle of Wight, UK in October/2015 and supported by the Imperial Centre for Inference and Cosmology (ICIC), Imperial College of London, UK, and by the Mullard Space Science Laboratory (MSSL) at the University College of London, UK. The IAA Cosmostatistics Initiative⁹ (COIN) is a non-profit organization whose aim is to nourish the synergy between astrophysics, cosmology, statistics, and machine learning communities. This work was written on the collaborative OVERLEAF platform¹⁰, made use of GITHUB¹¹ a web-

based hosting service and git version control software, DATAJOY¹² an on-line collaborative programming platform for PYTHON and R users, and SLACK¹³ a team collaboration platform.

References

- Abadi M. G., Moore B., Bower R. G., 1999, *MNRAS*, **308**, 947
 Abazajian K. N., et al., 2009, *ApJS*, **182**, 543
 Abraham R. G., van den Bergh S., 2001, *Science*, **293**, 1273
 Abraham R. G., et al., 1996, *ApJ*, **471**, 694
 Alam S., et al., 2015, *ApJS*, **219**, 12
 Alonso S., Coldwell G., Lambas D. G., 2014, *A&A*, **572**, A86
 Andreon S., Hurn M. A., 2010, *MNRAS*, **404**, 1922
 Antonucci R., 1993, *ARA&A*, **31**, 473
 Austin P. C., 2011, *Multivariate Behavioral Research*, **46**, 399
 Baldry I. K., Glazebrook K., Brinkmann J., Ivezić Ž., Lupton R. H., Nichol R. C., Szalay A. S., 2004, *ApJ*, **600**, 681
 Baldry I. K., Balogh M. L., Bower R. G., Glazebrook K., Nichol R. C., Bamford S. P., Budavari T., 2006, *MNRAS*, **373**, 469
 Baldwin J. A., Phillips M. M., Terlevich R., 1981, *PASP*, **93**, 5
 Barkhouse W. A., Yee H. K. C., López-Cruz O., 2009, *ApJ*, **703**, 2024
 Bhardwaj A., Kanbur S. M., Macri L. M., Singh H. P., Ngeow C.-C., Ishida E. E. O., 2016, *MNRAS*, **457**, 1644
 Birnboim Y., Dekel A., 2003, *MNRAS*, **345**, 349
 Blanton M. R., Roweis S., 2007, *AJ*, **133**, 734
 Blanton M. R., Eisenstein D., Hogg D. W., Schlegel D. J., Brinkmann J., 2005, *ApJ*, **629**, 143
 Bluck A. F. L., Ellison S. L., Patton D. R., Simard L., Mendel J. T., Teimoorinia H., Moreno J., Starkenburg E., 2014, preprint, ([arXiv:1412.3862](https://arxiv.org/abs/1412.3862))
 Booth C. M., Schaye J., 2013, *Scientific Reports*, p. 1738
 Boselli A., Cortese L., Boquien M., Boissier S., Catinella B., Gavazzi G., Lagos C., Saintonge A., 2014, *A&A*, **564**, A67
 Brinchmann J., Charlot S., White S. D. M., Tremonti C., Kauffmann G., Heckman T., Brinkmann J., 2004, *MNRAS*, **351**, 1151
 Calvi R., Poggianti B. M., Fasano G., Vulcani B., 2012, *MNRAS*, **419**, L14
 Cattaneo A., et al., 2009, *Nature*, **460**, 213
 Cattaneo A., Mamon G. A., Warnick K., Knebe A., 2011, *A&A*, **533**, A5
 Cid Fernandes R., Stasińska G., Schlickmann M. S., Mateus A., Vale Asari N., Schoenell W., Sodré L., 2010, *MNRAS*, **403**, 1036
 Cisternas M., Sheth K., Salvato M., Knapen J. H., Civano F., Santini P., 2015, *ApJ*, **802**, 137
 Coelho P., Gadotti D. A., 2011, *ApJ*, **743**, L13
 De Souza R. S., et al., 2015a, *Astronomy and Computing*, **12**, 21
 De Souza R. S., Hilbe J. M., Buelens B., Riggs J. D., Cameron E., Ishida E. E. O., Chies-Santos A. L., Killedar M., 2015b, *MNRAS*, **453**, 1928
 Dekel A., Birnboim Y., 2006, *MNRAS*, **368**, 2
 Doi M., et al., 2010, *AJ*, **139**, 1628
 Dressler A., 1980, *ApJ*, **236**, 351
 Duarte M., Mamon G. A., 2015, *MNRAS*, **453**, 3848
 Elliott J., de Souza R. S., Krone-Martins A., Cameron E., Ishida E. E. O., Hilbe J., 2015, *Astronomy and Computing*, **10**, 61
 Fabian A. C., 2012, *ARA&A*, **50**, 455
 Feigelson E. D., Babu G. J., 1992, *ApJ*, **397**, 55
 Ferrarese L., Merritt D., 2000, *ApJ*, **539**, L9
 Fujita Y., 2004, *PASJ*, **56**, 29
 Gao L., White S. D. M., Jenkins A., Stoehr F., Springel V., 2004, *MNRAS*, **355**, 819
 Gebhardt K., et al., 2000, *ApJ*, **539**, L13
 Gelman A., Hill J., 2007, Data analysis using regression and multilevel/hierarchical models. Analytical methods for social research, Cambridge University Press, New York
 Gelman A., Rubin D. B., 1992, *Statist. Sci.*, **7**, 457

⁹ <https://asaip.psu.edu/organizations/iaa/iaa-working-group-of-cosmostatistics>

¹⁰ www.overleaf.com

¹¹ <https://github.com>

¹² www.getdatajoy.com

¹³ <https://slack.com>

- Gilmour R., Gray M. E., Almaini O., Best P., Wolf C., Meisenheimer K., Papovich C., Bell E., 2007, *MNRAS*, **380**, 1467
- Gómez P. L., et al., 2003, *ApJ*, **584**, 210
- Goto T., Yamauchi C., Fujita Y., Okamura S., Sekiguchi M., Smail I., Bernardi M., Gomez P. L., 2003, *MNRAS*, **346**, 601
- Gunn J. E., Gott III J. R., 1972, *ApJ*, **176**, 1
- Hardin J. W., Hilbe J. M., 2012, *Generalized Linear Models and Extensions*, 3rd edn. StataCorp LP
- Häring N., Rix H.-W., 2004, *ApJ*, **604**, L89
- Harris K., et al., 2016, *MNRAS*, **457**, 4179
- Hashimoto Y., Oemler Jr. A., Lin H., Tucker D. L., 1998, *ApJ*, **499**, 589
- Hilbe J., 2009, *Logistic Regression Models*. Chapman & Hall/CRC Texts in Statistical Science, Taylor & Francis, <https://books.google.com/books?id=eJcMIAAACA>
- Hilbe J., 2014, *Modeling Count Data*. Cambridge University Press
- Ho D., Imai K., King G., Stuart E., 2007, *Political Analysis*, **15**, 199–236
- Ho D. E., Imai K., King G., Stuart E. A., 2011, *Journal of Statistical Software*, **42**, 1
- Hogg D. W., et al., 2004, *ApJ*, **601**, L29
- Hopkins P. F., Hernquist L., Cox T. J., Di Matteo T., Robertson B., Springel V., 2006, *ApJS*, **163**, 1
- Hubble E., 1929, *Proceedings of the National Academy of Sciences*, **15**, 168
- Ishibashi W., Fabian A. C., 2016, *MNRAS*, **457**, 2864
- Ishida E. E. O., de Souza R. S., 2013, *MNRAS*, **430**, 509
- Isobe T., Feigelson E. D., Akritas M. G., Babu G. J., 1990, *ApJ*, **364**, 104
- Jogee S., 2006, in Alloin D., ed., *Lecture Notes in Physics*, Berlin Springer Verlag Vol. 693, *Physics of Active Galactic Nuclei at all Scales*. p. 143 ([arXiv:astro-ph/0408383](https://arxiv.org/abs/astro-ph/0408383)), [doi:10.1007/3-540-34621-X_6](https://doi.org/10.1007/3-540-34621-X_6)
- Kauffmann G., et al., 2003, *MNRAS*, **346**, 1055
- Kauffmann G., White S. D. M., Heckman T. M., Ménard B., Brinchmann J., Charlot S., Tremonti C., Brinkmann J., 2004, *MNRAS*, **353**, 713
- Kaviraj S., Shabala S. S., Deller A. T., Middelberg E., 2015, *MNRAS*, **454**, 1595
- Kelly B. C., 2007, *ApJ*, **665**, 1489
- Kereš D., Katz N., Weinberg D. H., Davé R., 2005, *MNRAS*, **363**, 2
- Kereš D., Katz N., Davé R., Fardal M., Weinberg D. H., 2009, *MNRAS*, **396**, 2332
- Kewley L. J., Dopita M. A., Sutherland R. S., Heisler C. A., Trevena J., 2001, *ApJ*, **556**, 121
- Khabiboulline E. T., Steinhardt C. L., Silverman J. D., Ellison S. L., Mendel J. T., Patton D. R., 2014, *ApJ*, **795**, 62
- Kormendy J., Kennicutt Jr. R. C., 2004, *ARA&A*, **42**, 603
- Krongold Y., Dultzin-Hacyan D., Marziani P., 2001, *AJ*, **121**, 702
- Land K., et al., 2008, *MNRAS*, **388**, 1686
- Larson R. B., Tinsley B. M., Caldwell C. N., 1980, *ApJ*, **237**, 692
- Lenz D., Flöer L., Kerp J., 2016, *A&A*, **586**, A121
- Li Y., Bryan G. L., Ruszkowski M., Voit G. M., O’Shea B. W., Donahue M., 2015, *ApJ*, **811**, 73
- Lietzen H., Heinämäki P., Nurmi P., Liivamägi L. J., Saar E., Tago E., Takalo L. O., Einasto M., 2011, *A&A*, **535**, A21
- Lintott C. J., et al., 2008, *MNRAS*, **389**, 1179
- Lynden-Bell D., 1969, *Nature*, **223**, 690
- Magorrian J., et al., 1998, *AJ*, **115**, 2285
- Maraston C., 2005, *MNRAS*, **362**, 799
- Martini P., 2004, in Storch-Bergmann T., Ho L. C., Schmitt H. R., eds, *IAU Symposium Vol. 222, The Interplay Among Black Holes, Stars and ISM in Galactic Nuclei*. pp 235–241 ([arXiv:astro-ph/0404426](https://arxiv.org/abs/astro-ph/0404426)), [doi:10.1017/S1743921304002170](https://doi.org/10.1017/S1743921304002170)
- Miller C. J., Nichol R. C., Gómez P. L., Hopkins A. M., Bernardi M., 2003, *ApJ*, **597**, 142
- Moles M., Marquez I., Perez E., 1995, *ApJ*, **438**, 604
- Moore B., Katz N., Lake G., Dressler A., Oemler A., 1996, *Nature*, **379**, 613
- Nelder J. A., Wedderburn R. W. M., 1972, *Journal of the Royal Statistical Society, Series A, General*, **135**, 370
- Orban de Xivry G., Davies R., Schartmann M., Komossa S., Marconi A., Hicks E., Engel H., Tacconi L., 2011, *MNRAS*, **417**, 2721
- Page M. J., et al., 2012, *Nature*, **485**, 213
- Pimbblet K. A., 2011, *MNRAS*, **411**, 2637
- Pimbblet K. A., Shabala S. S., Haines C. P., Fraser-McKelvie A., Floyd D. J. E., 2013, *MNRAS*, **429**, 1827
- Raichoor A., Andreon S., 2012, *A&A*, **543**, A19
- Raichoor A., Andreon S., 2014, *A&A*, **570**, A123
- Reines A. E., Volonteri M., 2015, *ApJ*, **813**, 82
- Roediger E., Hensler G., 2005, *A&A*, **433**, 875
- Roediger E., et al., 2015, *ApJ*, **806**, 103
- Schawinski K., Thomas D., Sarzi M., Maraston C., Kaviraj S., Joo S.-J., Yi S. K., Silk J., 2007, *MNRAS*, **382**, 1415
- Schawinski K., et al., 2010, *ApJ*, **711**, 284
- Sereno M., 2016, *MNRAS*, **455**, 2149
- Shin M.-S., Ostriker J. P., Ciotti L., 2012, *ApJ*, **745**, 13
- Singh R., et al., 2013, *A&A*, **558**, A43
- Smolčić V., 2009, *ApJ*, **699**, L43
- Somerville R. S., Hopkins P. F., Cox T. J., Robertson B. E., Hernquist L., 2008, *MNRAS*, **391**, 481
- Stasińska G., Cid Fernandes R., Mateus A., Sodré L., Asari N. V., 2006, *MNRAS*, **371**, 972
- Stasińska G., et al., 2008, *MNRAS*, **391**, L29
- Stasińska G., Costa-Duarte M. V., Vale Asari N., Cid Fernandes R., Sodré L., 2015, *MNRAS*, **449**, 559
- Strateva I., et al., 2001, *AJ*, **122**, 1861
- Tremaine S., et al., 2002, *ApJ*, **574**, 740
- Trevisan M., Mamon G. A., Khosroshahi H. G., 2016, preprint, ([arXiv:1604.07726](https://arxiv.org/abs/1604.07726))
- Urry C. M., Padovani P., 1995, *PASP*, **107**, 803
- Veilleux S., Osterbrock D. E., 1987, *ApJS*, **63**, 295
- Villarreal B., Korn A. J., 2014, *Nature Physics*, **10**, 417
- Von der Linden A., Wild V., Kauffmann G., White S. D. M., Weinmann S., 2010, *MNRAS*, **404**, 1231
- Wada K., 2004, in *Carnegie Observatories Astrophysics Series, Vol. 1: Co-evolution of Black Holes and Galaxies*. Ed. L. C. Ho (Cambridge: Cambridge University Press), 186 ([arXiv:astro-ph/0308134](https://arxiv.org/abs/astro-ph/0308134))
- Yang X., Mo H. J., van den Bosch F. C., Pasquali A., Li C., Barden M., 2007, *ApJ*, **671**, 153

APPENDIX A: POSTERIORES

We display in Figure A1 the computed posteriors for the β coefficients in Equation confidence interval.

APPENDIX B: JAGS MODEL

In the following, we show how to translate the graphical model in Fig. 4 into JAGS using the R2JAGS package. Note that JAGS uses precision $\tau = 1/\sigma^2$ in place of variance σ^2 . The whole script, which one should run from within R, to load the data and recover the coefficients displayed in Tab. 1 is given below:

```
#####
# JAGS Script in R
# Required libraries
library(R2jags)
#Data
data<-read.csv("https://goo.gl/ppMoS1",header=T)

X <- model.matrix( ~ logM200 + r_r200, data = data)
K <- ncol(X) #Number of Predictors
y <- data$bpT #Response variable
n <- length(y) #Sample size
gal <- as.numeric(data$zoo) #Galaxy type
```

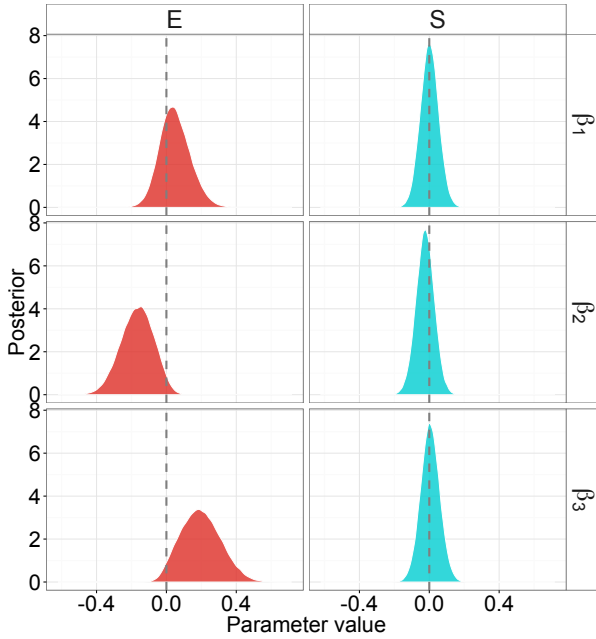


Figure A1. Computed posterior for the β coefficients of Fig. 4 From top to bottom β stands for: Intercept, $\log M_{200}$, and r/r_{200} for elliptical (left panel) and spiral (right panel) galaxies respectively.

```
model.file = textConnection(jags_model),
n.chains = nc,
n.thin = th,
n.iter = s,
n.burnin = burn)
```

```
# Partial output
print(jags_fit,intervals=c(0.025, 0.975),
digits=3)
```

An example of the output of the JAGS model is shown below.

```
#####
Inference for Bugs model, fit using jags,
3 chains, each with 50000 iterations
      mu.vect sd.vect   2.5%  97.5%
beta[1,1]  0.049  0.088  -0.112  0.238
beta[2,1] -0.169  0.094  -0.356  0.003
beta[3,1]  0.197  0.115  -0.010  0.428
beta[1,2]  0.003  0.052  -0.100  0.107
beta[2,2] -0.024  0.052  -0.130  0.075
beta[3,2]  0.006  0.054  -0.099  0.113
#####
```

This paper has been typeset from a $\text{\TeX}/\text{\LaTeX}$ file prepared by the author.

```
#JAGS data
jags_data <- list(Y=y,
                 N = n,
                 X=X,
                 gal=gal)

#Model
jags_model<-"model{
#Shared hyperpriors for beta
tau ~ dgamma(1e-3,1e-3) #Precision
mu ~ dnorm(0,1e-3) #mean
#Diffuse prior for beta
for(j in 1:2){
for(k in 1:3){
beta[k,j]~dnorm(mu,tau)
}}
# Likelihood
for(i in 1:N){
Y[i] ~ dbern(pi[i])
logit(pi[i]) <- eta[i]
eta[i] <- beta[1,gal[i]]*X[i,1]+
beta[2,gal[i]]*X[i,2]+
beta[3,gal[i]]*X[i,3]
}"}

# Monitor this parameter
params <- c("beta")
# Generate initial values
inits <- function () {
list(beta = matrix(rnorm(6,0, 0.01),ncol=2))}

# Run MCMC
burn = 2*10^4 #Burn-in samples
s = 5*10^4 #Number of samples
nc = 3 #Number of mcmc
th = 10 #Thinning value

jags_fit <- jags(
data = jags_data,
inits = inits,
parameters = params,
```